MATERIALE PLASTICE
https://revmaterialeplastice.ro
https://doi.org/10.37358/Mat.Plast.1964

Influence of Shell Structure on the Tensile Strength of Fused Filament Fabrication Models

CHEN WANG[1,2]*, JINGYAO LI[1,2], XIAOWEN WANG[1,2], QING CHU[1,2], TIANYI WANG[1,2]
[1] Nanjing Forestry University, College of Furnishings and Industrial Design, Nanjing Jiangsu, 159 Longpan Road, Nanjing Forestry University, Nanjing, Jiangsu Province, China
[2] Jiangsu Co-Innovation Center of Efficient Processing and Utilization of Forest Resources, Jiangsu, 159 Longpan Road, Nanjing Forestry University, Nanjing, Jiangsu Province, China

Abstract: *The shell, as the main structure of 3D printed fused filament fabrication (FFF) models, plays a key role in the tensile strength of FFF models. In order to optimise the structural parameters of the shell and improve the tensile strength of FFF models, especially those printed with low-density infill. In this paper, polylactic acid (PLA) filament was selected as the printing material, and the influence of shell structural parameters (shell texture angle, shell layer height, and shell thickness) on the tensile strength of FFF models was investigated by one-way and orthogonal tests. The results of the one-way test show that the tensile strength of the FFF models increases as the shell texture angle decreases, the shell layer height decreases, and the shell thickness increases. Orthogonal test results show that the shell structure parameters affect the tensile strength of the FFF models in the following degree: shell thickness > shell texture angle > shell layer height. The optimised shell structure parameters are: shell texture angle of 0°, shell layer height of 0.1 mm, shell thickness of 2.0 mm, and the tensile strength of the FFF models is the largest with this optimised parameter, which is 19.68 MPa.*

Keywords*: Shell structure, 3D printing, FFF model, Tensile strength*

1. Introduction

In recent years, 3D printing technology has been widely used in industrial manufacturing. Among all kinds of 3D printing technologies, Fused Filament Fabrication (FFF) has shown stronger competitiveness because of its simple process principle, low material cost, and wide range of applications, etc. The process principle of FFF technology is as follows: Plastic filament is transported to the nozzle through the filament supplying mechanism, and heated up to a molten state in the nozzle. Driven by the processing data, the nozzle moves according to the cross-sectional contour of the model and selectively deposits the molten filament on the printing platform, where it cools rapidly to form a solid sheet. Subsequently, the nozzle is moved up a certain height (i.e. layer height) and the next layer of the cross-sectional contour is deposited, and so on, resulting in a 3D-printed FFF model [1-4].

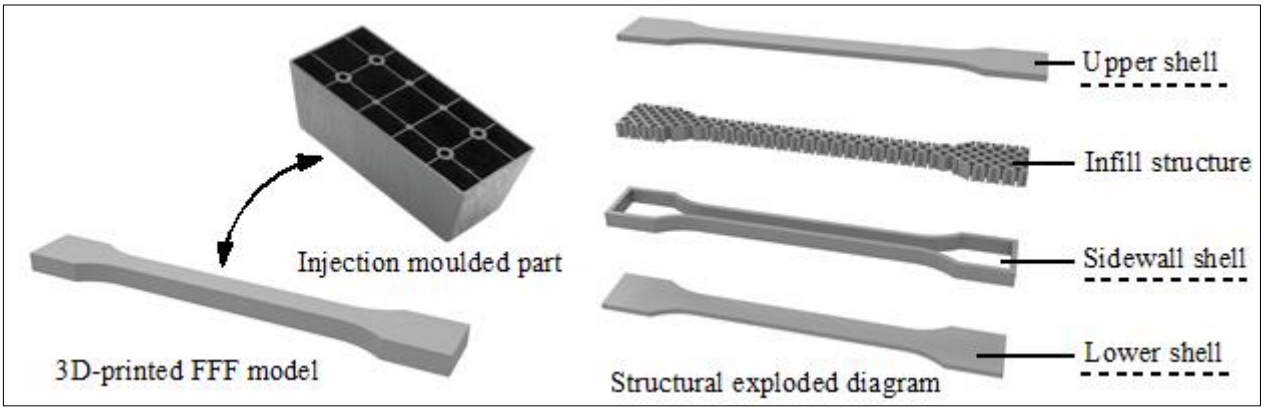

Figure 1. Exploded diagram of 3D-printed FFF model

*email: 996869559@qq.com

Inspired by the structure of injection moulded parts, the 3D-printed FFF model is analogous to injection moulded parts. In the structural design of injection moulded parts, the shell and the stiffeners together affect the structural strength of the injection moulded part [5]. The FFF model is disassembled, and from the exploded diagram (Figure 1), the FFF model can be divided into two parts: the shell and the infill, and the shell is further divided into the upper shell, the lower shell and the sidewall shell. The shell of the FFF model is equivalent to the outer shell of the injection moulded part, while the infill is equivalent to the stiffener of the injection moulded part [6-8].

In order to effectively improve the tensile strength of FFF models, strengthening the shell structure and strengthening the infill structure are the two main directions. The current research on the direction of strengthening the shell structure is less, and mainly focuses on the direction of strengthening the infill structure, i.e., optimising the infill parameters to achieve the improvement of the tensile strength of the FFF models [9-11]. However, the shell, as the main structure of the FFF model, surrounds the perimeter of the model and plays a key role in the tensile strength of the model, especially for the FFF models with low-density infill, the shell mainly bears the tensile load because the area of the shell in any cross-section perpendicular to the tensile load is larger than the infill area [12-14]. Therefore, in this paper, from the direction of strengthening the shell structure, the shell texture angle, shell layer height, and shell thickness among the shell structural parameters were selected as the research objects, and the influence of the shell texture angle, shell layer height, and shell thickness on the tensile strength of the FFF models was analysed through the one-way test and orthogonal test. It provides a reference for optimising the shell structural parameters and improving the tensile strength of the FFF models.

2. Materials and methods

2.1. Materials

The PLA filament (1.75 mm diameter, White color, Anycubic, Shenzhen, China) was used for additive manufacturing by FFF technology.

2.2. Specimen preparation

Referring to the dumbbell-shaped specimen specified in the ASTM D-638 standard, the 3D model shown in Figure 2a was designed by SolidWorks software (Dassault Systemes, Education Version 2016, Paris, France). A Kobra 3D printer (0.4 mm nozzle diameter, X-Y-Z printing, Anycubic, Shenzhen, China) was used to fabricate the FFF models, and PLA filament was selected as the material. The conventional printing parameters were set as follows: nozzle temperature of 220°C, hot bed temperature of 60°C, extrusion rate of 100%, and printing speed of 50 mm/min [15].

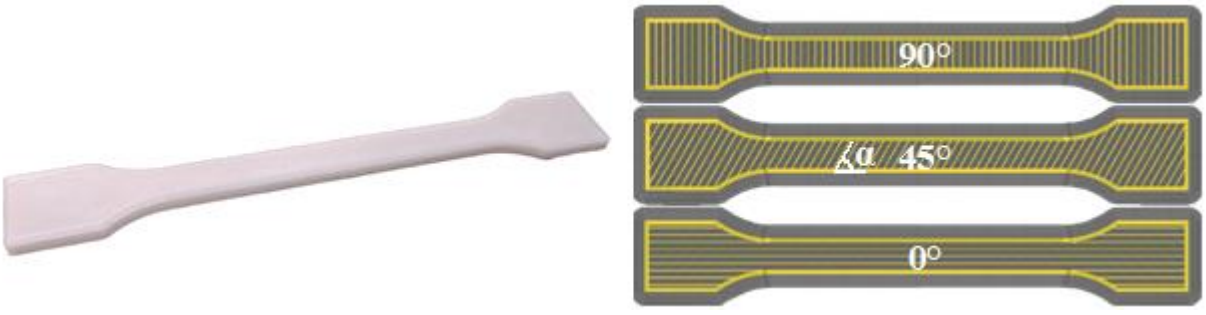

(a) Dumbbell-shaped specimen (b) Shell texture angle

Figure 2. Dumbbell-shaped tensile specimen

The settings of the shell structure parameters are specified later in this paper. The shell texture angle refers to the angle α between the surface filaments of the upper and lower shell and the long side of the dumbbell-shaped specimen (Figure 2b); the shell layer height refers to the distance that the nozzle moves each time when printing the shell cross-sectional contour in layers [16]; and the shell thickness refers to

the thickness values of the upper shell, the lower shell, and the sidewall shell. In order to make the FFF model more balanced with the force of each part of the shell in tensile conditions, the upper shell, lower shell, and sidewall shell in the present test are all of equal thicknesses [17].

2.3. Performance test

Referring to the tensile test method stipulated in ASTM D-638 standard, A universal mechanical testing machine (20 KN, AG-X, Shimadzu, Kyoto, Japan) was used to test the tensile strength of dumbbell-shaped specimens, and the test was carried out in a quasi-static loading condition, with a loading speed of 2 mm/min, at a room temperature of 20°C [18].

3. Results and discussions

3.1. Influence of shell texture angle on the tensile strength of FFF models

Tensile tests were carried out on the FFF models with 0°, 45° and 90° texture angle under the conditions of 0.1 mm shell layer height and 2.0 mm shell thickness to investigate the influence of shell texture angle on the tensile strength of the FFF models. As seen in Figure 3, the tensile strength of the FFF models with 0°, 45° and 90° texture angle are 18.68 MPa, 16.13 MPa and 13.35 MPa. With the decreases of the shell texture angle, the tensile strength of the FFF models increases.

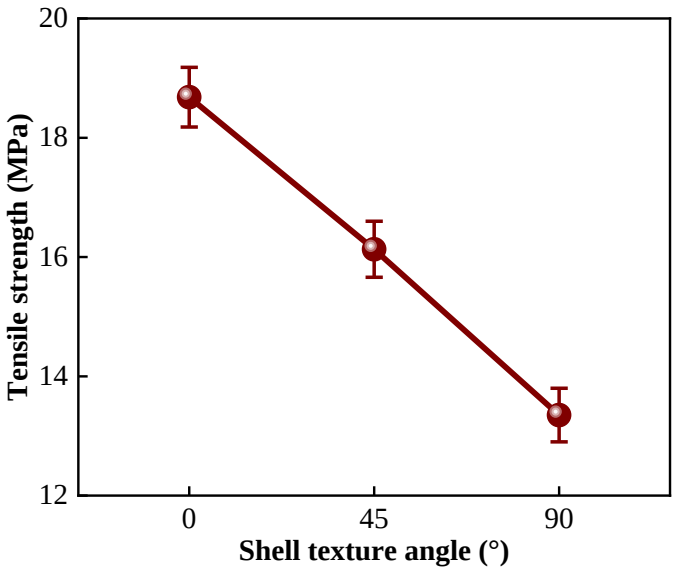

Figure 3. Influence of shell texture angle on the tensile strength of FFF models

This is because during the printing process, there is a temperature difference between the molten filament extruded from the nozzle and the solidified filament, and the rapid heat transfer causes the molten filament to cool down rapidly, weakening the diffusion of PLA molecules at the bonding interface [19]. As a result, the macromolecular chains of the molten filament could not cross the bonding interface, and only a small part of the chain segments were entangled with the chain segments of the solidified filament [20]. As a result, the molecular entanglement density at the bonding interface is lower than that inside the filament body, which is macroscopically manifested as the structural strength at the filament bonding interface is lower than that of the filament body [21]. When the shell texture angle is 90°, the direction of tensile force is parallel to the direction of the filament body, the filament body directly bears the load, and the tensile strength of the FFF models is the largest; when the shell texture angle is 0°, the direction of tensile force is perpendicular to the direction of the filament body, and the weak filament bonding interface bears the load, and the tensile strength of the FFF models is the smallest;

when the shell texture angle is 45°, the filament body and the filament bonding interface bear the load at the same time, and the tensile strength of the FFF models is in the middle.

3.2. Influence of shell layer thickness on the tensile strength of FFF models

Tensile tests were carried out on the FFF models with 0.1 mm, 0.2 mm and 0.3 mm shell layer height under the conditions of 0° shell texture angle and 2.0 mm shell thickness to investigate the influence of shell layer height on the tensile strength of the FFF models. As shown in Figure 4, the tensile strength of the FFF models with 0.1 mm, 0.2 mm and 0.3 mm shell layer height are 18.68 MPa, 16.92 MPa and 15.57 MPa. With the decreases of the shell layer height, the tensile strength of the FFF models increases.

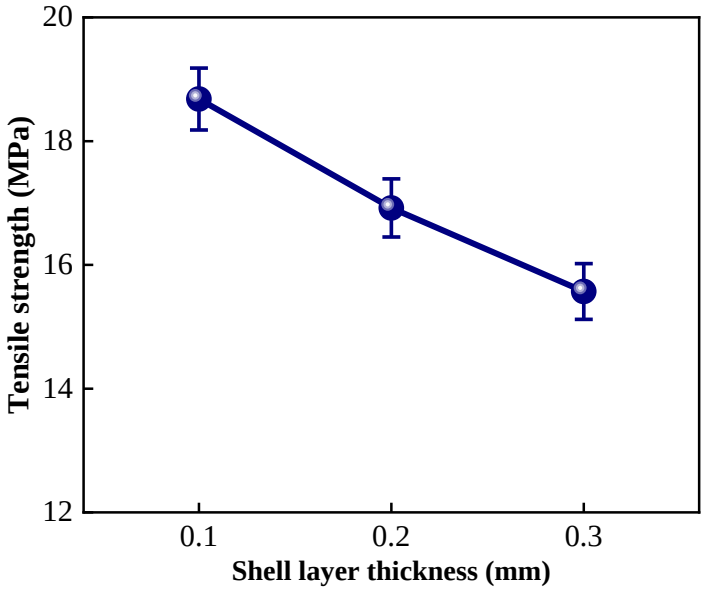

Figure 4. Influence of shell layer thickness on the tensile strength of FFF models

Due to the elliptical cross-sectional shape of the molten filament extruded from the nozzle of an FFF printer, there are usually “seams” in the fusion area with neighbouring filaments in both the vertical and horizontal directions [22]. As a structural defect, “seams” are prone to stress concentrations and lead to damage of the specimen [23]. As the shell layer height decreases, the extrusion pressure of the nozzle increases in the vertical direction, resulting in full extrusion of the molten filament at the interlayer bonding interface. Through the extrusion effect, the horizontal flow of the molten filament was generated, which filled the “seams” and promoted the entanglement of PLA molecular chain segments at the bonding interface, thus effectively improving the interlayer bonding performance of the shell and increasing the tensile strength of the FFF models.

3.3. Influence of shell thickness on the tensile strength of FFF models

Tensile tests were carried out on the FFF models with 1.2 mm, 1.6 mm and 2.0 mm shell thicknesses under the conditions of 0° shell texture angle and 0.1 mm shell layer height to investigate the influence of shell thickness on the tensile strength of the FFF models. As seen in Figure 5, the tensile strength of the FFF models with 1.2 mm, 1.6 mm and 2.0 mm shell thicknesses are 12.65 MPa, 15.33 MPa and 18.68 MPa. With the increases of shell thickness, the tensile strength of the FFF models increases.

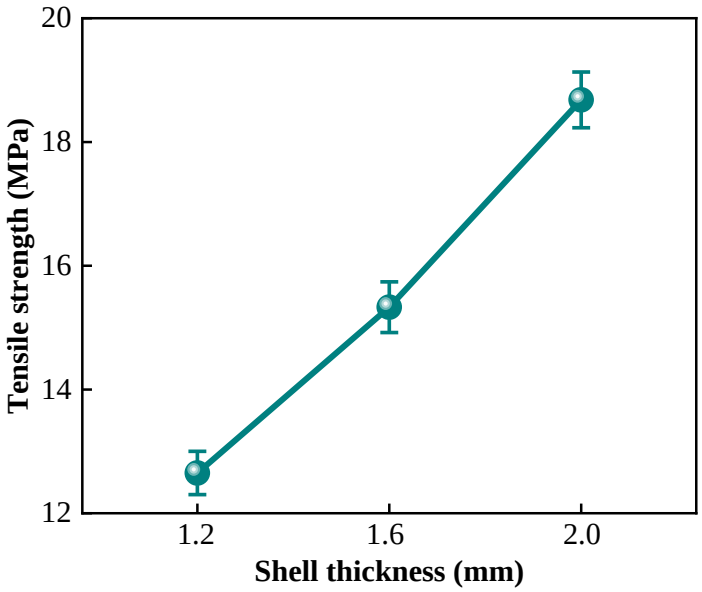

Figure 5. Influence of shell thickness on the tensile strength of FFF models

This is because the FFF tensile models belong to equal cross-section rods, and as the shell thickness increases, it makes the shell area on any cross-section of the FFF models increases, which correspondingly results in a decrease of the infill area, resulting in an increase of the shell volume and a decrease of the infill volume for the overall model. Since the shell texture is at 0° angle, the filament body bears the load, while the infill texture is at 45° angle, the filament body and the filament bonding interface bear the load at the same time [24]. However, the weak filament bonding interface is easy to be damaged, which results in the tensile strength of the infill structure is lower than that of the shell structure [25]. Therefore, as the shell thickness increases, the volume of the shell structure with higher tensile strength increases and the tensile strength of the FFF models increases.

Orthogonal test

Design of the Orthogonal Test

Shell texture angle, shell layer height, and shell thickness were selected as orthogonal test influencing factors, and a three-factor, three-level orthogonal test was designed, with the factor level table shown in Table 1, where Factor A represents shell texture angle, Factor B represents shell layer height, and Factor C represents shell thickness.

Table 1. Orthogonal test factor level table

Levels	Influencing factors		
	Shell texture angle (*A*)/°	Shell layer height (*B*)/mm	Shell thickness (*C*)/mm
1	0	0.1	1.2
2	45	0.2	1.6
3	90	0.3	2.0

L9 (3^3) orthogonal test table was selected, and nine groups of FFF models were fabricated on the 3D printer, and when each group of FFF models was cooled down to room temperature (20°C), tensile tests were carried out to test their tensile strength, and the results of the tests are shown in Table 2. As can be seen in Table 2, the model tensile strength T_1 obtained by group 1 test was the largest, which was 19.68 MPa, and that of the model tensile strength T_7 obtained by group 7 test was the smallest, which was 7.23 MPa.

Table 2. Orthogonal test results table

Group number (*i*)	*A*/°	*B*/mm	*C*/mm	Tensile strength (T_i) / MPa
1	0	0.1	2.0	19.68
2	0	0.2	1.6	15.12
3	0	0.3	1.2	11.36
4	45	0.3	1.6	11.81
5	45	0.2	1.2	11.49
6	45	0.1	2.0	16.13
7	90	0.3	1.2	7.23
8	90	0.2	2.0	12.85
9	90	0.1	1.6	12.04

Range analysis

The data from the tests in Table 2 were analysed and the results are shown in Table 3. In Table 3, K_i represents the sum of tensile strength at different levels of the same factor; M_i is the mean value of K_i; R (Range) value is the difference between the maximum and minimum values of the same factor.

Table 3. Range analysis table

Calculation result	*A*	*B*	*C*
K_1	46.16	47.85	30.08
K_2	39.43	39.46	38.97
K_3	32.12	39.30	47.85
M_1	15.39	15.95	10.03
M_2	13.14	13.15	12.99
M_3	10.71	13.10	15.95
R	4.68	2.85	5.92

From Table 3, it can be seen that the shell texture angle of A_1 (0°) is the best, because its K_1 value is the largest, so in the range of 0~90°, the tensile strength of the FFF models with 0° shell texture angle is the largest; the shell layer height of B_1 (0.1 mm) is the best, because its K_1 value is the largest, so in the range of 0.1~0.3 mm, the tensile strength of the FFF models with 0.1 mm shell layer height is the largest; the shell thickness of C_3 (2.0 mm) is the best, because its K_3 value is the largest, so in the range of 1.2~2.0 mm, the tensile strength of the FFF models with 2.0 mm shell thickness is the largest.

Comparing the R (Range) value, it can be seen that $R_C > R_A > R_B$, so the influence of shell structure parameters on the tensile strength of the FFF models is as follows: shell thickness > shell texture angle > shell layer height. The optimised shell parameter is $A_1B_1C_3$, i.e., the shell texture angle is 0°, the shell layer height is 0.1 mm, and the shell thickness is 2.0 mm. With this optimised parameter, the tensile strength of the FFF models is the largest and is 19.68 MPa, which is consistent with the results of the one-way test and verifies the reliability of the test.

4. Conclusions

In this paper, PLA filament was selected as the printing material and dumbbell-shaped specimens were printed by FFF technology. The influence of shell structure parameters (shell texture angle, shell layer height, and shell thickness) on the tensile strength of the FFF models was investigated. The results of the one-way test show that the tensile strength of the FFF models increases as the shell texture angle decreases, the shell layer height decreases, and the shell thickness increases.

A three-factor, three-level orthogonal test was carried out by selecting shell texture angle, shell layer height, and shell thickness as the influencing factors, and the results of the orthogonal test showed that the influence of shell structural parameters on the tensile strength of the FFF models was as follows: shell thickness > shell texture angle > shell layer height. The optimised shell structure parameters are:

shell texture angle of 0°, shell layer height of 0.1 mm, shell thickness of 2.0 mm, and the tensile strength of the FFF models under these optimised parameters is the largest, which is 19.68 MPa.

References

1.YANG, Z. Z., FENG, X. H., XU, M., RODRIGUE, D., Printability and properties of 3D printed poplar fiber/polylactic acid biocomposites. *BioResources*, 2022, 16(2), 2774-2788.
2.YANG, L., LIU, D., GUO, R., JI, Z. Y., WANG, X. L., SHI, X. Y., Flexibility of Diels-Alder reversible covalent bonds in fused deposition modeling 3D printing: Bonding and de-bonding. *Polymer*, 2023, 266:125637.
3.YILMAZ, M., YILMAZ, N. F., KALKAN, M. F., Rheology, crystallinity, and mechanical investigation of interlayer adhesion strength by thermal annealing of polyetherimide (PEI/ULTEM 1010) parts produced by 3D printing. *Journal of Materials Engineering and Performance*, 2022, 31(12), 9900-9909.
4.ZOU, Y. M., XIA, Y. X., YAN, X. X., Effect of melamine formaldehyde resin encapsulated UV acrylic resin primer microcapsules on the properties of UV primer coating. *Polymers*, 2024, 16(16), 2308.
5. WANG, Y. Q., LIU, Z. G., GU, H. W., CUI, C. Z., HAO, J. B., Improved mechanical properties of 3D-printed SiC/PLA composite parts by microwave heating. *Journal of Materials Research*, 2019, 34(20), 3412-3419.
6. ZHANG, R., YU, L. G., CHEN, K., XUE, P., JIA, M. Y., HUA, Z. T., Amelioration of interfacial properties for CGF/PA6 composites fabricated by ultrasound-assisted FDM 3D printing. *Composites Communications*, 2023, 39(20):101551.
7. YU, S. L., ZHENG, Q., CHEN, T. Y., ZHANG, H. L., CHEN, X. R., Consumer personality traits vs. their preferences for the characteristics of wood furniture products. *BioResources*, 2023, 18(4), 7443-7459.
8. DING, T. T., YAN, X. X., ZHAO, W. T., Effect of urea–formaldehyde resin–coated colour–change powder microcapsules on performance of waterborne coatings for wood surfaces. *Coatings*, 2022, 12(9), 1289.
9. LUO, M., TIAN, X. Y., SHANG, J. F., ZHU, W. J., LI, D. C., QIN, Y. J., Impregnation and interlayer bonding behaviours of 3D-printed continuous carbon-fiber-reinforced poly-ether-ether-ketone composites. *Composites Part A-Applied Science and Manufacturing*, 2019, 121, 130-138.
10. WANG, L., HAN, Y., YAN, X. X., Effects of adding methods of fluorane microcapsules and shellac resin microcapsules on the preparation and properties of bifunctional waterborne coatings for basswood. *Polymers*, 2022, 14(18), 3919.
11. ZOU, Y. M., PAN, P., YAN, X. X., Comparative analysis of performance of water-based coatings prepared by two kinds of anti-bacterial microcapsules and nano-silver solution on the surface of andoung wood. *Coatings*, 2023, 13(09), 1518.
12. HAN, Y., YAN, X. X., ZHAO, W. T., Effect of thermochromic and photochromic microcapsules on the surface coating properties for metal substrates. *Coatings*, 2022, 12(11), 1642.
13. ZHOU, C. M., HUANG, T., LIANG, S., Smart home R&D system based on virtual reality. *Journal of Intelligent & Fuzzy Systems*, 2020, 40(2), 3045-3054.
14. LI, R. R., CHEN, J. J., WANG, X.-D., Prediction of the color variation of moso bamboo during CO2 laser thermal modification. *BioResources*, 2020, 15(3), 5049-5057.
15. MO, X. F., ZHANG, X. H., FANG, L., ZHANG, Y., Research progress of wood-based panels made of thermoplastics as wood adhesives. *Polymers*, 2022, 14(1), 98.
16. YU, S. L., WU, Z. H., Research on the influence mechanism of short video communication effect of furniture brand: based on ELM model and regression analysis. *BioResources*, 2024, 19(2), 3191-3207.
17. LI, W. B., YAN, X. X., ZHAO, W. T., Preparation of crystal violet lactone complex and its effect on discoloration of metal surface coating. *Polymers*, 2022, 14(20), 4443.

18.QI, Y. Q., SUN, Y., ZHOU, Z. W., HUANG, Y., LI, J. X, LIU, G. Y., Response surface optimization based on freeze-thaw cycle pretreatment of poplar wood dyeing effect. *Wood Research*, 2023, 68(2), 293-305.
19.FENG, X. H., YANG, Z. Z., WANG, S. Q., WU, Z. H., The reinforcing effect of lignin-containing cellulose nanofibrils in the methacrylate composites produced by stereolithography. *Polymer Engineering and Science*, 2022(9), 2968-2976.
20. LIU, Q., GU, Y., XU, W., LU, T., LI, W., FAN, H., Compressive properties of green velvet material used in mattress bedding. *Applied Sciences*, 2021, 11(23), 11159.
21.ZHOU, J. C., XU, W., Toward interface optimization of transparent wood with wood color and texture by silane coupling agent. *Journal of Materials Science*, 2022, 57(10), 5825-5838.
22.YANG, L., HAN, T. Q., LIU, Y. X., Yin, Q., Effects of vacuum heat treatment and wax impregnation on the color of pterocarpus macrocarpus kurz. *BioResources*, 2021, 16(1), 954-963.
23.ZHOU, C. M., HUANG, T., LUO, X., KANER, J., Reorganisation and construction of an age-friendly smart recreational home system: based on function-capability match methodology. *Applied Sciences-Basel*, 2023, 13(7), 9783.
24.LIU, Y., HU, J., WU, Z. H., Fabrication of coatings with structural color on a wood surface. *Coatings*, 2020, 10(1), 32.
25.WANG, Q., FENG, X. H., LIU, X. Y., Functionalization of nanocellulose using atom transfer radical polymerization and applications: A review. *Cellulose*, 2023, 30, 8495-8537.

Manuscript received: 22.07.2024